



Co-precipitation synthesis, structural characterization and fluorescent analysis of Nd³⁺ doped Y₃Al₅O₁₂ and Yb₃Al₅O₁₂ nanocrystallines

Taiping Xie¹ · Li Zhang² · Jiankang Wang¹ · Taiping Xie³ · Quanxi Zhu¹ · Xiaodong Zhang¹

Received: 10 October 2018 / Accepted: 3 December 2018 / Published online: 7 December 2018
© Springer Science+Business Media, LLC, part of Springer Nature 2018

Abstract

Nd³⁺, as one of the most important rare-earth (RE) ion, has been playing a significant role in pumping the infrared (IR) light. Depending on different synthesis strategies, doping content, and crystal lattice, however, Nd³⁺ always shows different IR intensity. In this work, we have fabricated two series of Nd³⁺ doped nanocrystallines that share with the same crystal structure, i.e., Nd³⁺ doped Y₃Al₅O₁₂ (YAG) and Yb₃Al₅O₁₂ (YbAG), through using the co-precipitation synthesis method while the ammonium bicarbonate as the precipitant agent. To reveal the influence of the synthesis conditions (e.g., synthetic temperature and pH value) on structural and fluorescent properties of Nd³⁺ doped YAG and YbAG nanocrystallines, several techniques have been performed in this work, including the X-ray diffraction (XRD), scanning electron microscopy (SEM), thermogravimetric-differential scanning calorimeter (TG-DSC), Fourier transform infrared (FT-IR) spectroscopy, Raman and fluorescent spectroscopy spectra. Our results reveal that the optimal synthesis conditions are 1000 °C and pH 8 for YAG:Nd³⁺ and 900 °C and pH 9 for YbAG:Nd³⁺. Moreover, we also find the optimal Nd³⁺ doping contents of the YAG:Nd³⁺ and YbAG:Nd³⁺ nanocrystallines are 3% and 1.5%, which correspond to the strongest fluorescent intensity upon excitation at 808 nm and 980 nm, respectively. Typically, we reveal that substitution of Y with Yb ions could allow to enhancing the Nd³⁺ fluorescent intensity upon excitation at 808 nm. This work provides new insights into designing excellent crystal materials that can allow us to realize the laser transparent ceramics.

1 Introduction

In the recent years, great attentions have been paid to the laser crystal materials that base on the crystal host of Y₃Al₅O₁₂ (YAG) [1–3], leading to a variety of feasible strategies (e.g., CW and pulse triggered operations) that can realize the commonly-used solid-state laser source [4, 5]. Although other laser materials, such as ScVO₄ [6, 7], Ln₂O₃ (Ln=Y, Sc, Lu) [8], MF₂ (M=Ca, Sr, Ba) [9] and MgO [10], have become available, we notice that most of them cannot work without using the Nd³⁺ ion as the activator. In addition,

during the process of laser light realization, a transparent ceramic, featuring the advantages of large size, easily-control shape, economic-cost, high doping concentration, good optical homogeneity and multiple functions, is highly desirable. This is because it can play the necessity role of medium function, typically when we take into account the laser output and adjusted-Q value during the synthesis process. When compared to the frequently-used preparation methods (e.g., solvothermal [6], sol-gel [11] and solid-state reaction methods [12]), it is generally believed that the simpler preparation method for laser medium material would be the better.

The past decades have witnessed that Nd³⁺ doped YAG laser has been widely accepted as the most commonly-recognized solid-state laser light source [13–23], but the shortcomings, such as the Nd³⁺ doped content-induced fluorescent quenching upon excitation at 980 nm and 808 nm, high synthesis temperature and low pump light absorption ability [12, 13, 24], are the main obstacles, which will greatly hinder the Nd³⁺ doped YAG laser materials toward some upfront cutting-edge applications (e.g., high-power gun). As a result, great efforts have been made over the past years, aiming to upgrade the IR fluorescent properties

✉ Taiping Xie
deartaiping@163.com

¹ Chongqing Key Laboratory of Extraordinary Bond Engineering and Advanced Materials Technology (EBEAM), Yangtze Normal University, Chongqing 408100, China

² Chongqing Academy of Metrology and Quality Inspection, Chongqing 401123, China

³ Department of Environmental Engineering, Zhejiang University, Hangzhou 310058, China

of Nd³⁺ doped YAG laser materials through increasing the Nd³⁺ doping content.

With the rapid development of InGaAs laser diode (LD) pump, researches find that another type of RE Yb³⁺ ion featured a simple energy level structure can be used as a promise active ion to address the above Nd³⁺ content-induced fluorescent quenching problem. Because of the advantages such as the high quantum efficiency upon excitation at 980 nm and 808 nm, long fluorescent life, low non-radiation-relaxation-induced heat load and non-excited absorption [15–17], the Yb³⁺ ion can exhibit its ability to work together with Nd³⁺ and then to enhance the Nd³⁺ fluorescent intensity [18–20]. Remarkably, after comparing the ionic radii of Yb³⁺ ion with that of Y³⁺ ion at the same coordinate number, we can easily find that their ionic radii are very close with each other. For example, at the coordinate numbers of 8, the Yb³⁺ and Y³⁺ ions exhibit the ionic radii of 0.985 Å and 1.019 Å [22, 23], respectively. As a result, substitution of Y³⁺ ion with Yb³⁺ ion in the YAG become possible, allowing to expecting the Nd³⁺ fluorescent properties can be enhanced in the Yb/YAG related crystal materials but still keep the laser behavior analogous to the YAG:Nd³⁺. Enlightened by the above discussion, we thus have tried the Nd³⁺ doped YbAG and some mediate (Y,Yb)AG counterparts. In view of the strong absorption ability of Yb³⁺ ion at 808 nm and 980 nm, the improved Nd³⁺ output fluorescent intensity, resulting from the energy transfer from Yb³⁺ to Nd³⁺, could be expected. This may further give rise to conquering the Nd³⁺ concentration induced fluorescent quenching. All in all, if one wants to achieve the Nd³⁺ fluorescent intensity yet lower sintering temperature, using the Yb³⁺ ion to increase the Nd³⁺ absorption efficiency is a good choice. So, co-doping the Yb³⁺ ion may improve the fluorescent properties of Nd³⁺ doped YAG.

In this work, we designed and fabricated two series of Nd³⁺ doped YAG and YbAG, by taking advantages of the co-precipitation method. To study the preparation conditions, the influence factors, such as the pH, synthesis temperature and Nd³⁺ doped concentration, were studied. To check the structural and fluorescent properties, characterization techniques including the XRD, SEM, Raman spectroscopy, TG-DSC, FT-IR and fluorescent spectroscopy, were carried out. Our findings revealed that the optimal Nd³⁺ doped contents of the YAG:Nd³⁺ and YbAG:Nd³⁺ nanocrystallines upon excitation at 808 nm and 980 nm were 3% and 1.5%, respectively. The results were different from the case of YbAG:Nd³⁺ upon excitation 808 nm, where we found that there was no Nd³⁺ doping content-induced fluorescent quenching within the Nd³⁺ doped range of 0–5.0%. This work developed a new type of YAG materials that could allow us to realize the laser transparent ceramic and, thus, will be an important work in the laser field.

2 Experimental section

2.1 Sample synthesis

Firstly, we designed the chemical compositions of (Y,Yb)_{3-x}Al₅O₁₂:Nd_x³⁺, where the x values were 0.5%, 1.0%, 1.5%, 2.0%, 2.5%, 3.0%, 3.5%, and 5.0%. Then, on the basis of the raw materials of Y₂O₃ (99.99%), Yb₂O₃ (99.99%), Al₂O₃ (99.99%) and Nd₂O₃ (99.99%), we had carefully calculated the amount of each raw materials according to the above compositions. Specifically, we first dissolved the raw materials of Y₂O₃, Yb₂O₃, Al₂O₃ and Nd₂O₃ into 50 mL of 5 mol/L diluted HNO₃, followed by adding 20 mL of 2 mol/L Al(NO₃)₃·9H₂O solution. Then, 10 g of ammonium bicarbonate (NH₄HCO₃) and 5 g of ammonium sulfate ((NH₄)₂SO₄) were added into the solution, allowing them to act as the precipitating agent and dispersing agent, respectively. Noted that the reverse co-precipitation method required a homogeneous mixing and the adding speed of the solution needed slower than 2 mL/min, the aim of which was to prevent the blistering and occurrence of the unwanted reactions. During the process, the pH values of titrated solution were controlled from 6, 7, 8, 9 and to 10. After titrated, an absolute ethanol with a volume ratio of 1:10 total solutions were added. With 20 h aging, the achieved solutions were filtered and rinsed by deionized water and absolute ethanol solutions three times. Then, the precursors were achieved after drying the filtered precipitate at 120 °C for 20 h. Finally, we fired the powders in air by using a ceramic crucible at 800 °C, 900 °C, 1000 °C, 1100 °C, and 1200 °C. After cooling to room temperature, the final YAG:Nd³⁺ and YbAG:Nd³⁺ nanocrystallines were achieved.

2.2 Characterizations

The thermal properties of YAG:Nd³⁺ and YbAG:Nd³⁺ were recorded on a NETZSCH STA409PC thermogravimetric-Differential Scanning Calorimeter(TG-DSC). The α-Al₂O₃ was used as the reference. The heating rate and range were set to 10 K/min and 25–1250 °C, respectively. A Japan Rigaku Ultima IV X-ray diffraction (XRD) analyzer, working with the CuK_α radiation source, scanning range of 10–70° and rate of 10°/min, radiation wavelength of 1.5405 Å, X-ray tube voltage of 40 kV and current of 20 mA, was used to record the XRD of samples. The morphologies, surface chemical groups and microstructure of samples were recorded on a JEOL JSM-6701F field emission scanning electron microscope (SEM) and PerkinElmer Fourier transform infrared (FT-IR) spectroscopy. Raman spectroscopy equipped with a 514.5 nm

Jobin–Yvon HR800 microscopic argon laser was used to record molecular features of samples. Fluorescent spectra of samples were recorded on a JY Fluorolog-3-tau fluorescent spectrometer equipped with an 808 nm and 980 nm pump excitation source.

3 Results and discussion

3.1 XRD and SEM analysis

Figure 1a, b(i, ii) gives the influence of synthesis temperature (a) and pH value (b) on the crystal phase variation of Nd^{3+} doped YAG and YbAG nanocrystallines. As can be seen, when the synthesis temperatures and pH values are greater than 800 °C and 7, the main XRD peaks of samples match well with the peaks derived from ICSD card No. 67102 and No. 20861 with the increase of the temperature and the pH value, the XRD intensity features an initial increase and then a subsequent decrease. Meanwhile, the XRD shape and full width half maximum (FWHM) become sharper and narrower with increasing of temperature and pH value, as reflected by the tendency variation. As a result, the optimal temperature and pH value are determined to 1000 °C and 8 for Nd^{3+} doped YAG, while 900 °C and 9

for Nd^{3+} doped YbAG. Furthermore, we also calculated the cell parameters of all samples based on the XRD results. The dependence of temperature and pH value on the cell parameters is shown in Fig. 1a, b(iii). As can be seen, the cell parameters (a , b , c) and cell volumes (V) seem to change little as compared to the ICSD card No. 67102 and No. 20861 cell parameters as compared to the standard lattice parameters (a , b , c) and cell volumes (V) of bulk YAG and YbAG crystals (i.e., $a=b=c=12.0163$ Å, and $V=1734.92$ Å³ for YAG; $a=5.8302$ Å, $b=14.7634$ Å, $c=6.2212$ Å, and $V=448.80$ Å³ for YbAG), in particular when compared to those solid solutions which always involve the crystal ions with different ionic radii at the same coordination [24, 25]. This is because when the contents of Yb^{3+} , Y^{3+} and Nd^{3+} ions in the YAG and YbAG crystal host are fixed, changing the temperature and pH value do not induce the change of their ionic radii. As a result, little change of the crystal lattice cell parameters can be observed when the temperature and pH value are changed. Of course, due to the different ions radii between Yb^{3+} ($R=1.14$ Å, $CN=8$), Y^{3+} ($R=1.019$ Å, $CN=8$) and Nd^{3+} ($R=1.109$ Å, $CN=8$) ions, doping of YAG and YbAG with the Nd^{3+} ion can allow the Nd^{3+} ion to substitute the Yb^{3+} and Y^{3+} ions rather than the Al sites ($R=0.39$ Å, $CN=4$; $R=0.535$ Å, $CN=6$) [22, 23]. As a result, doping of YAG and YbAG with the Nd^{3+} ion

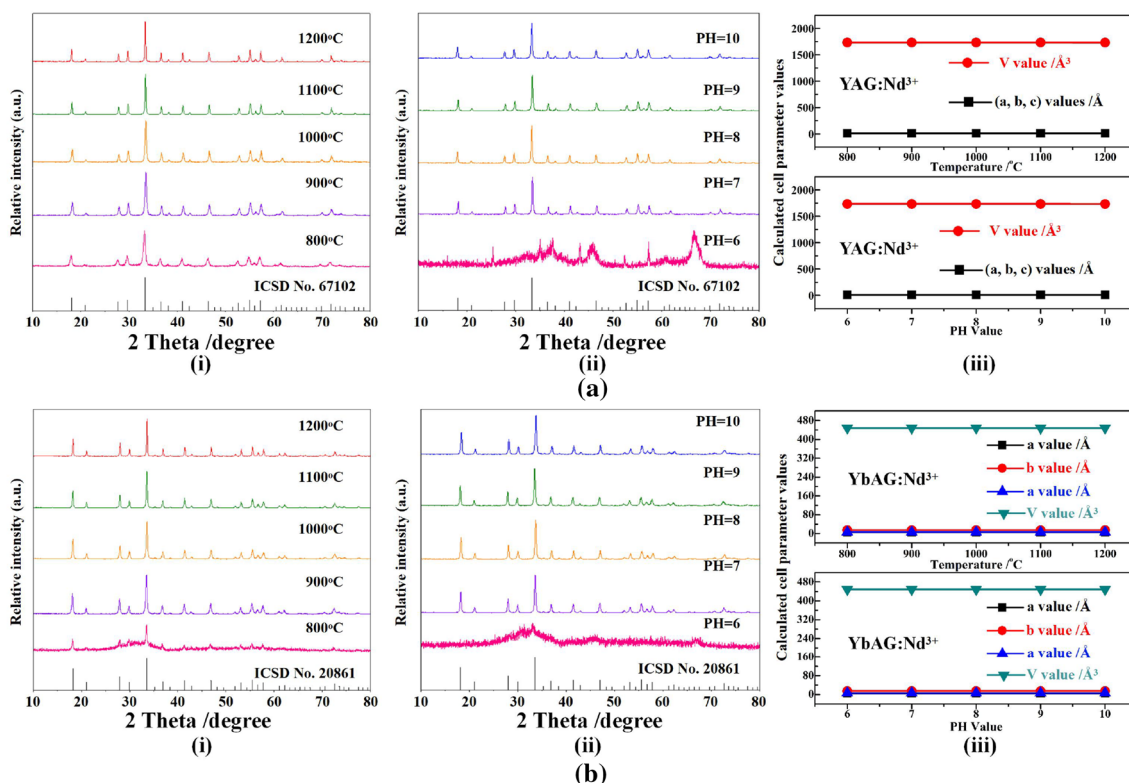


Fig. 1 Influence of temperature (a)(i, ii) and pH value (b)(i, ii) on the crystal phase variation of Nd^{3+} doped YAG and YbAG nanocrystallines; dependence of temperature (a)(iii) and pH value (b)(iii) on the crystal cell parameters of Nd^{3+} doped YAG and YbAG nanocrystallines

almost cannot induce the change of lattice parameters (a , b , c) and cell volumes (V) of YAG:Nd^{3+} and YbAG:Nd^{3+} . Such lattice parameters and cell volumes of YAG and YbAG before and after doped with Nd^{3+} can also reveal the successful incorporation of Nd^{3+} into the YAG and YbAG crystal lattice.

Except for the above XRD characterizations, we also used the SEM technique to observe the influence of the synthesis temperatures and pH values on the microstructure variation, and results are shown in Fig. 2. Clearly, in Fig. 2a, the temperature and pH value of Nd^{3+} doped YAG sample that correspond to the best nanocrystal behaviour are 1000 °C and 8, respectively. The average particle size is ~75 nm (Fig. 2c), with excellent crystalline and good size distribution. This indicates the synthesis condition should be the best condition to render the Nd^{3+} fluorescence. In addition, when the temperature is either less or greater 1000 °C, particles with incomplete crystallization, larger grain and closed pore appear. For the Nd^{3+} doped YbAG (Fig. 2b), several particles with uniform size distribution at 50 nm, well dispersed and good crystallization are observed when the synthesis temperature and pH value are 900 °C and 9. When the temperature and pH value are less or greater than 900 °C and 9, Nd^{3+} doped YbAG particles are either unevenness, closed pores, non-fully formed or irregular morphologies. Such crystal information tells us that the interface reflection and refraction of light that can result in the decrease of the optical transmittance may appear in the Nd^{3+} doped YbAG when the temperature and pH value are not 900 °C and 9. This is not good news for the transparent ceramic

and the laser output. However, the TEM results at least can somewhat reflect the XRD information (Fig. 1). That is, what the optimal temperature and pH value can allow to achieving the best transparent Nd^{3+} doped YAG and YbAG nanocrystallines.

3.2 TG-DSC and FT-IR spectral analysis

In view of the significant influence of synthesis temperature on the crystallizing process, we carried out the TG-DSC measurement on the Nd^{3+} doped YAG and YbAG samples in order to understand their intrinsic thermal decomposition mechanism. The TG-DSC results are shown in Fig. 3. We can see from the TG-DSC curves that the Nd^{3+} doped YAG and YbAG samples after gradually dried is close to 41% and 63% weight as compared to their respective initial weight. Specifically, we loaded 3 mg of Nd^{3+} doped YAG and YbAG into the TG-DSC crucible and then heated them with gradually increasing the temperature. We can see that the TG curve of Nd^{3+} doped YAG experiences a rapid decrease of mass when the temperature is less 600 °C (Fig. 3a). This is due to thermal-induced loss of water, nitrate radical and hydroxyl and decomposition of ammonium and partial carbonate. Such observation is related to an exothermic peak within the range of 600–850 °C, as reflected by the DSC curve. This, as reflected by 7.2% weight loss (see the TG curve), is due to the decomposition of carbonate. For the exothermic peak at 920 °C, it is ascribed to the YAG crystallization phase. However, with further increasing the temperature, the TG curve is deviated, typically after 900 °C,

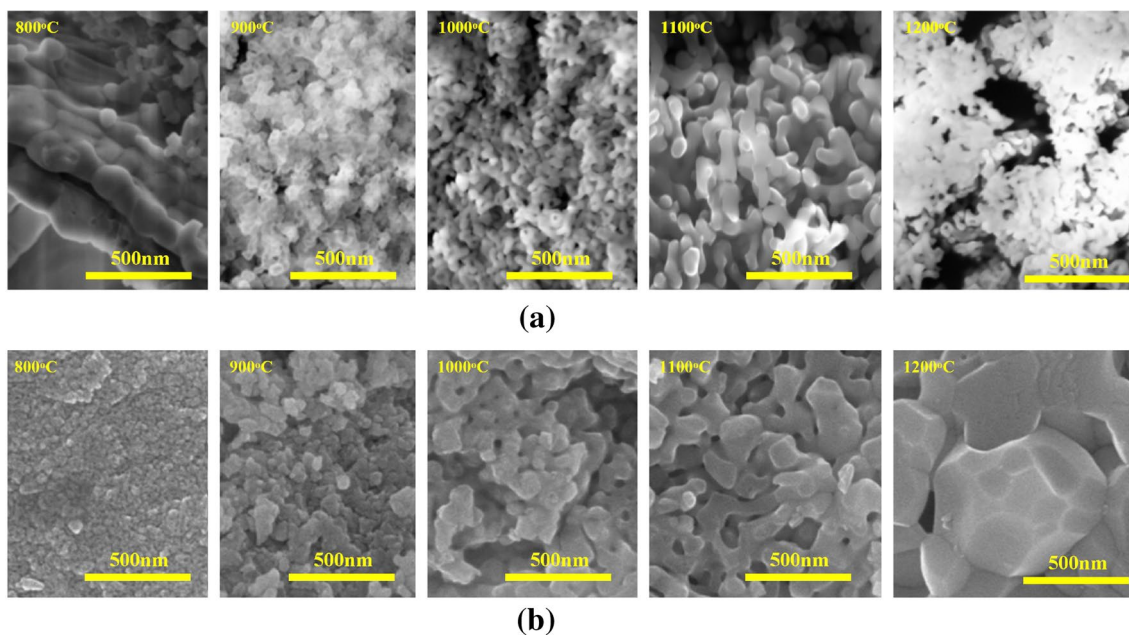


Fig. 2 TEM images of Nd^{3+} doped YAG (a) and YbAG (b) nanocrystallines prepared at different synthesis temperature

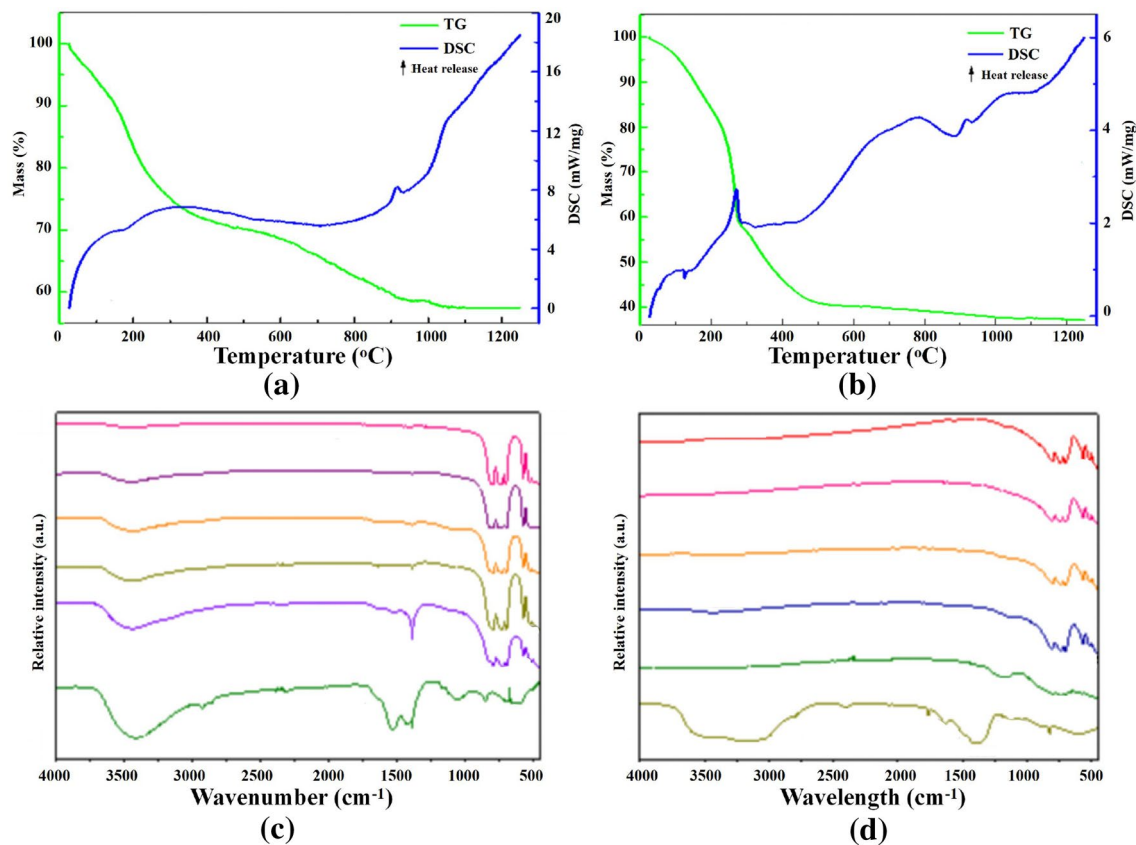


Fig. 3 TG-DSC curves of Nd³⁺ doped YAG (a) and YbAG (b) nanocrystallines; FT-IR spectra of Nd³⁺ doped YAG (a) and YbAG (b) nanocrystallines

which indicates the thermal decomposition process is over and the crystal structure of Nd³⁺ doped YAG become more stable when the temperature is greater than 900 °C. For Nd³⁺ doped YbAG sample (Fig. 3b), the TG-DSC curve is obviously different from that of Nd³⁺ doped YAG, where we can find its main reaction begins before 500 °C and almost 60% of weight has been lost when the temperature is up to 125 °C. This weight loss is due to the volatilization of physically-adsorbed water and crystal water (124.3 °C), the decomposition of NH⁴⁺ and carbonate (270.3 °C), and the release of NO³⁻ and OH⁻ groups. Within the temperature range of 700–1100 °C, there are several weak exothermic peaks, which are due to the weight loss resulted from the initial (785 °C), complete (918 °C) and crystal grain (1030 °C) forming process of YbAG. However, once the temperature is larger than 1050 °C, there is no obvious weight loss, indicating the fully-finished crystalline phase transition. Obviously, the crystallized processes of Nd³⁺ doped YAG and YbAG can be reflected by the TG-DSC results, and they are basically consistent the results we achieved in Figs. 1 and 2.

The FT-IR spectra of Nd³⁺ doped YAG and YbAG are also shown in Fig. 3. For bulk YAG (Fig. 3a), it exhibits a large number of FT-IR peaks, i.e., a weak peak at

3431 cm⁻¹ that corresponds to H–O–H bending vibration, several peaks at 846 cm⁻¹, 1420 cm⁻¹ and 1526 cm⁻¹ that are resulted from the asymmetric expansion and bending vibration of CO₃²⁻, and two peaks at 1385 cm⁻¹ and 668 cm⁻¹ that come respectively from the asymmetric vibration of NO₃⁻ and asymmetric absorption of SO₄²⁻. Other peaks, locating at 508 cm⁻¹, 566 cm⁻¹, 690 cm⁻¹, 720 cm⁻¹ and 785 cm⁻¹, are from the lattice vibrations and photons interaction of YAG. When the Nd³⁺ ions are doped into YAG, increasing the temperature does not change these peak positions, except for their intensity. Moreover, the FT-IR results of Fig. 3a further show that when the synthesis temperature is 900 °C, a peak located at 1385 cm⁻¹, which is from the asymmetric absorption vibration of NO₃⁻, can be detected. This indicates that there are still the NO₃⁻ groups, even though the YAG crystal phase has been formed. However, at this temperature, the purity-phase of Nd³⁺ doped YAG still cannot be achieved. As a result, the FT-IR results, together with the XRD and structural results of Figs. 1 and 2, tell us that the optimal temperature for Nd³⁺ doped YAG nanocrystalline is 1000 °C. In bulk YbAG (Fig. 3a), it shows more FT-IR absorption peaks than the bulk YAG. The peaks

at 3144 cm^{-1} and 1631 cm^{-1} are all from the stretching and bending vibrations of H–O–H, indicating the YAG surface contains a small amount of water. The absorption peaks at 600 cm^{-1} , 1129 cm^{-1} , 1763 cm^{-1} , and 2397 cm^{-1} are from the vibration of Al–O bond, SO_4^{2-} , NO_3^- , and HCO_3^- groups, respectively. In addition, the CO_3^{2-} groups have been also reflected by the FT-IR spectra, and the symmetric stretching and bending vibration directly lead to two FT-IR peaks at 1398 cm^{-1} and 824 cm^{-1} . When the synthesis temperature is up to $800\text{ }^\circ\text{C}$, two FT-IR peaks at 1163 cm^{-1} and 2327 cm^{-1} , which correspond to the vibration absorption of HCO_3^- and SO_4^{2-} groups, can still appear. Other peaks at 512 cm^{-1} , 563 cm^{-1} , 699 cm^{-1} , 738 cm^{-1} and 803 cm^{-1} , causing by the lattice vibrations and photons interactions of YbAG, are also observed. After doped with Nd^{3+} , the FT-IR peaks of the NO_3^- , HCO_3^- , CO_3^{2-} and SO_4^{2-} groups can be also clearly detected. The FT-IR results also indicate the optimal synthesis temperature is $900\text{ }^\circ\text{C}$.

3.3 Raman spectral analysis

After analyzed on the TG-DSC and FT-IR results, we carried out the Raman spectral analysis to the Nd^{3+} doped YAG and YbAG nanocrystallines. The Raman results of Nd^{3+} doped YAG and YbAG nanocrystallines are shown in Fig. 4. Figure 4a is the Raman spectra of Nd^{3+} doped YAG synthesized at the temperature of $1000\text{ }^\circ\text{C}$. Clearly, there are many Raman peaks at 162 cm^{-1} , 218 cm^{-1} , 260 cm^{-1} , 338 cm^{-1} , 370 cm^{-1} , 402 cm^{-1} , 716 cm^{-1} , 782 cm^{-1} , 980 cm^{-1} , 1046 cm^{-1} , 1122 cm^{-1} . After compared with previous works [26–28], these peaks are ascribed to the vibration of YAG that is mainly resulted from the mixing translational and rotational vibration of Y^{3+} ion and the asymmetric stretching vibration of AlO_4 groups. The dominated peak is located at 1122 cm^{-1} . For the Nd^{3+} doped YbAG sample achieved at $900\text{ }^\circ\text{C}$ (Fig. 4b), a series of Raman peaks, locating at 124 cm^{-1} , 158 cm^{-1} , 236 cm^{-1} , 258 cm^{-1} , 322 cm^{-1} , 362 cm^{-1} , 548 cm^{-1} , 706 cm^{-1} , 732 cm^{-1} , 800 cm^{-1} ,

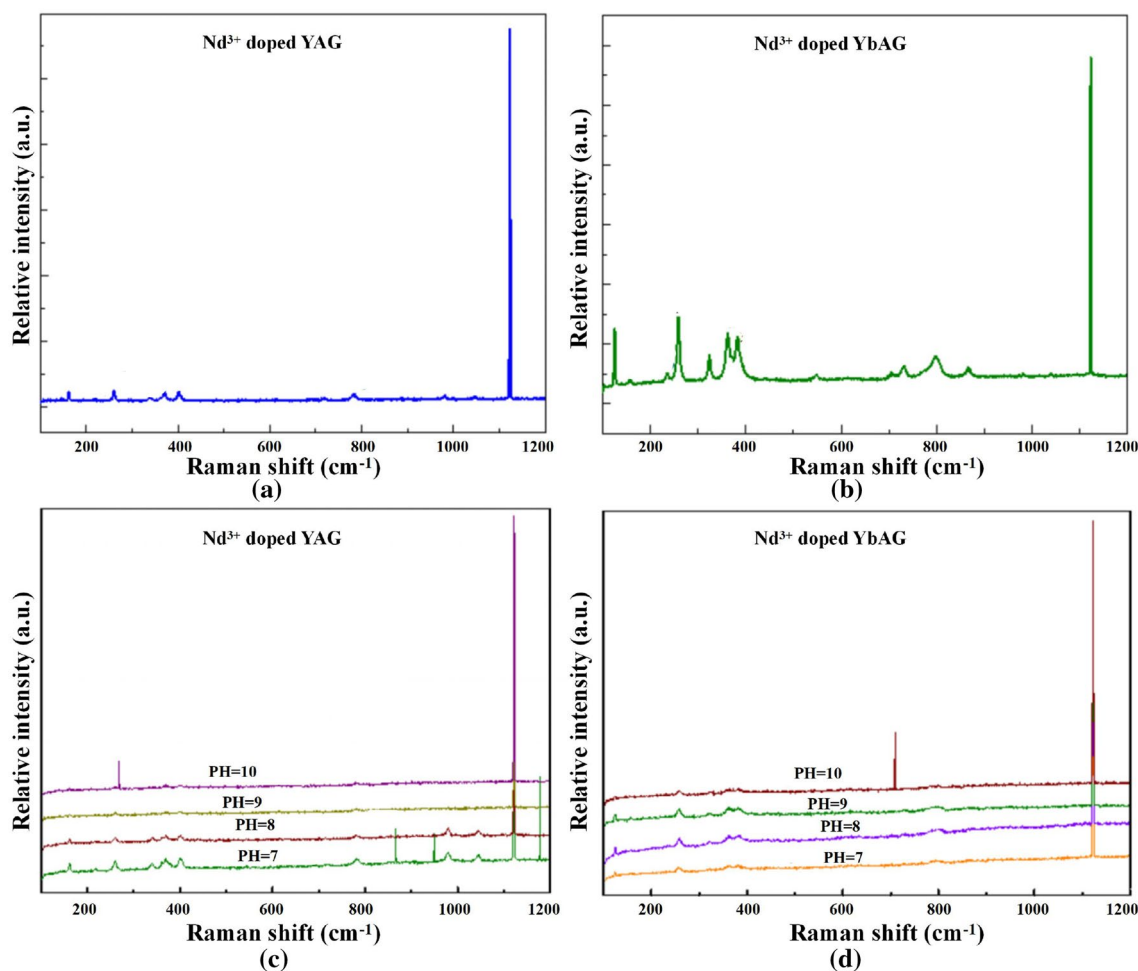


Fig. 4 Raman spectral curves of Nd^{3+} doped YAG (a) synthesized at $1000\text{ }^\circ\text{C}$ and YbAG (b) synthesized at $900\text{ }^\circ\text{C}$ nanocrystallines; Influence of pH value on the Raman spectra of the Nd^{3+} doped YAG (c) and YbAG (d) synthesized at $1000\text{ }^\circ\text{C}$ and $900\text{ }^\circ\text{C}$, respectively

866 cm^{-1} , and 1122 cm^{-1} , are observed. Similar to Nd^{3+} doped YAG sample, the Nd^{3+} doped YbAG sample also exhibits a dominated Raman peak at 1122 cm^{-1} . Among these peaks, except for the peak at 800 cm^{-1} that comes from the symmetry stretching and asymmetric bending vibration of AlO_4 , other peaks at 124 cm^{-1} , 158 cm^{-1} , 236 cm^{-1} , 258 cm^{-1} , 322 cm^{-1} , 362 cm^{-1} , 548 cm^{-1} , 706 cm^{-1} , 732 cm^{-1} , 866 cm^{-1} , and 1122 cm^{-1} are ascribed to the parallelism of Yb^{3+} lattice translational vibration, the rotational vibration and asymmetric stretching vibration of AlO_4 tetrahedral.

Figure 4c, d show the influence of pH value on the Raman spectra of Nd^{3+} doped YAG sample prepared at 1000 °C and Nd^{3+} doped YbAG sample prepared at 900 °C, respectively. In Fig. 4c, there are several sharp Raman peaks at 864 cm^{-1} , 950 cm^{-1} , 1178 cm^{-1} when the pH value is 7, and they are due to the bending vibration of C, the asymmetric stretching vibrations of O=N=O bond, the asymmetric stretching vibration of S=O bond, respectively. This indicates that there are still C, N and S elements resided in the YAG lattice due to the RE nitrate solution that can react with the ammonium bicarbonate precipitant in a neutral environment (pH 7). Except for the dominated peak at 1122 cm^{-1} , other peaks are very weak at the pH 9, indicating the incomplete crystallization at this pH value. A peak, locating at 267 cm^{-1} , appears when the pH value is 10, and it can be ascribed to the Al–O bending vibrations. With these Raman peaks, we can confirm the optimal pH value for Nd^{3+} doped YAG is 8. For Nd^{3+} doped YbAG (Fig. 4d), the pH range is 7–10. Raman signals are weak when pH is 7. The vibration intensity of molecular bond is not strong enough, thus exhibiting a poor sintering activity. Although the YbAG phases, as the XRD and TEM results revealed, can be formed, the YbAG crystal phase becomes not good enough under a neutral condition (pH 7). When pH is 10, a peak at 708 cm^{-1} , causing by the bending vibration of O=N=O and ON=O bands, can be seen, but Nd^{3+} doped YAG at this pH value does not reach a desirable phase-purity. When pH values is 8 and 9, distinguishable Raman peaks are observed, indicating this pH range is good for Nd^{3+} doped YAG phase. Obviously, Raman spectral results basically are consistent with the results of Figs. 1, 2 and 3. That is, the optimal pH values for Nd^{3+} doped YAG and YbAG are 8 and 8–9, respectively.

3.4 Fluorescent analysis

After determined the optimal synthesis temperature and pH value, we studied the fluorescent properties of Nd^{3+} doped YAG and YbAG samples upon pumping with the 808 nm and 980 nm NIR laser sources. The reason why we chose the 808 nm and 980 nm NIR wavelengths is because the Nd^{3+} and Yb^{3+} ions have been well known to

be good absorber to capture the 808 nm and 980 nm light for a long time, as witnessed by a large number of previous works and other commercial Nd^{3+} doped laser crystal materials such as $\text{Nd}^{3+}:\text{Y}_3\text{Al}_5\text{O}_{12}$ [3, 4], $\text{Yb}^{3+}:\text{Ln}_2\text{O}_3$ [8], $\text{Nd}:\text{YAG}-\text{BiBO}$ [12], $\text{SrWO}_4:\text{Nd}^{3+}$ [29], $\text{LuVO}_4:\text{Nd}^{3+}$ [30], and $\text{Nd}^{3+}:\text{PbWO}_4$ [31]. In Fig. 5a, a highest emission peak, locating at 1064 nm, can be detected in the Nd^{3+} doped YAG, which is ascribed to the ${}^4\text{F}_{3/2} \rightarrow {}^4\text{I}_{11/2}$ transition of Nd^{3+} [3, 4, 12, 13, 29–31]. Other peaks are very weak, and they have a negative impact on the luminous efficiency of crystals. With increasing the Nd^{3+} content [Fig. 5c (curve 1)], we can see that the emission intensity can increase initially and then decrease, showing the optimal Nd^{3+} doping content that corresponds to the strongest fluorescent intensity is 3%. With further increasing the Nd^{3+} content, the so-called fluorescent quenching appears. Such Nd^{3+} content-induced fluorescent quenching can also be frequently reported by other previous works [32, 33]. Figure 5b shows the fluorescent spectra of Nd^{3+} doped YbAG sample upon excitation at 980 nm. The spectral features are much simpler as compared to the spectra of Nd^{3+} doped YAG. There are only two main peaks at 1002 nm and 1030 nm and a weak peak at 992 nm, without the 1064 nm peak of Nd^{3+} . The 992 nm and 1002 nm peaks are from the Yb^{3+} transition of ${}^2\text{F}_{5/2} \rightarrow {}^2\text{F}_{7/2}$; while the 1030 nm peak is from the ${}^4\text{F}_{3/2} \rightarrow {}^4\text{I}_{11/2}$ transition of Nd^{3+} ion [3, 4, 12, 13, 29–35]. It indicates that upon excitation at 980 nm, the wavelength of which is from Yb^{3+} ion, can lead to the Nd^{3+} IR emission. Furthermore, when compared the results of Fig. 5b with that of Fig. 5a, we can find with the help of Yb^{3+} absorption the IR fluorescent intensity of Nd^{3+} ion can be enhanced greatly. The optimal Nd^{3+} content that corresponds to the strongest intensity is 1.5% (the curve 2 of Fig. 5c). Once the excitation wavelength is 808 nm, the Nd^{3+} doped YbAG sample exhibits three Nd^{3+} unique fluorescent peaks, i.e., 970 nm, 1004 nm, and 1030 nm. The dominated peak is located at 1030 nm. Unlike Fig. 5a and b, Fig. 5c reveals that increasing the Nd^{3+} doping content from 0 to 5% does not decrease the fluorescent intensity, which indicates that the $\text{YbAG}:\text{Nd}^{3+}$ does not exhibit the so-called concentration-induced fluorescent quenching. We conclude that this is due to the fact that substitution of Y ions with Yb ions can increase the limitation of the Nd^{3+} fluorescence, thereby overcoming the Nd^{3+} fluorescent quenching at the range of 0–5% Nd^{3+} content and enhancing the Nd^{3+} fluorescent intensity at the same time. Furthermore, on the basis of the fluorescent results, we can also conclude that the Nd^{3+} ions have successfully entered into the YAG and YbAG crystal lattices when we consider the fact that bulk YAG and YbAG crystals cannot show the IR fluorescence upon excitation at 808 nm and 980 nm. The fluorescent results are obviously consistent with our XRD analysis results.

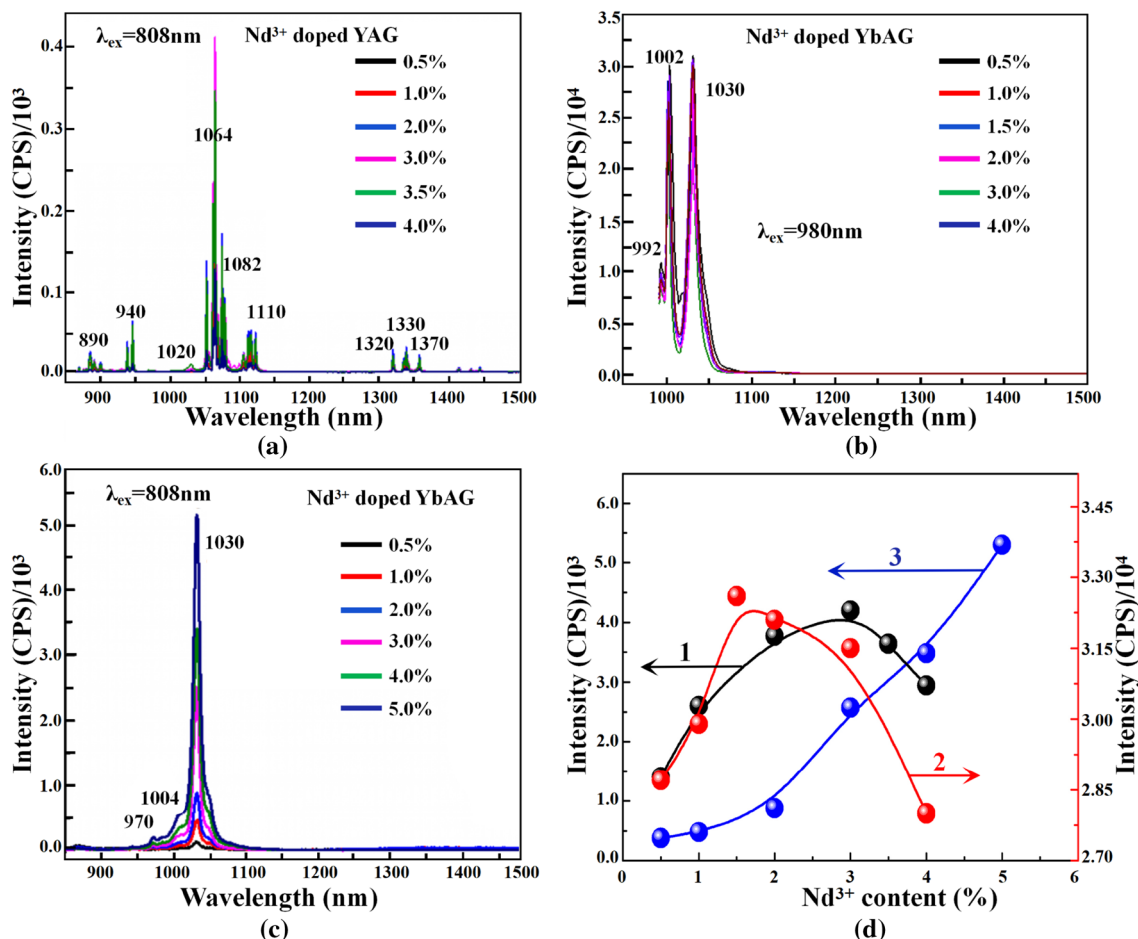


Fig. 5 Fluorescent spectra of Nd³⁺ doped YAG upon excitation at 808 nm (a), Nd³⁺ doped YbAG upon excitation at 980 nm (b) and 808 nm (c), and (d) dependence of Nd³⁺ doping content on the flu-

orescent intensity for Nd³⁺ doped YAG upon excitation at 808 nm (curve 1), Nd³⁺ doped YbAG upon excitation at 980 nm (curve 2) and 808 nm (curve 3), respectively

4 Conclusions and outlook

In this work, we had used the RE Nd³⁺ ion as the activator while the Y₃Al₅O₁₂ (YAG) and Yb₃Al₅O₁₂ (YbAG) as the crystal host to successfully fabricate two series of Nd³⁺ doped IR nanocrystallines that shared with the same crystal structure, i.e., Nd³⁺ doped Y₃Al₅O₁₂ (YAG) and Yb₃Al₅O₁₂ (YbAG). The co-precipitation method was involved to use the ammonium bicarbonate as the precipitant agent. In order to achieve the optimal synthesis conditions, we changed the synthesis temperature and pH value and studied their influence on the structural and fluorescent properties of Nd³⁺ doped YAG and YbAG. On the basis of the experimental results derived from several characterization techniques such as XRD, SEM, TG-DSC, FT-IR, Raman and fluorescent spectroscopy, we had determined the optimal synthesis conditions, i.e., 1000 °C and pH 8 for YAG:Nd³⁺ and 900 °C and pH 9 for YbAG:Nd³⁺. Furthermore, we found the optimal Nd³⁺ doping contents of the

YAG:Nd³⁺ and YbAG:Nd³⁺ nanocrystallines that corresponded respectively to the strongest fluorescent intensity upon excitation at 808 nm and 980 nm were 3% and 1.5%, respectively. These obviously were different from the case of YbAG:Nd³⁺ upon excitation at 808 nm, where we found there was no Nd³⁺-content-induced fluorescent quenching. Since the downconversion luminescence by pumping the short-wavelength into long-wavelength process and their related applications such as white LED device [36–39] while the upconversion luminescence refers to a nonlinear optical anti-Stokes process that can convert lower frequency incident photons (e.g., NIR light) into higher-energy photons (e.g., visible and even ultraviolet light) through several intermediate long-lived energy states of lanthanide ions [40–42], this work, which also refers to the upconversion luminescence, could provide new insights into designing more excellent materials that can allow us to realize the laser transparent ceramics.

Acknowledgements We acknowledge the financial support from youth research talents' growth support program of Yangtze Normal University. We would like to appreciate our associates, especially Xiulong Lan, Chunlan He, Yuan Peng, Songli Liu, and Yajing Wang for their valuable contributions to our research program. We gratefully acknowledge many important contributions from the researchers of all reports cited in our paper.

Compliance with ethical standards

Conflict of interest The authors declare that they have no conflict of interest.

References

1. I. Akio, L.A. Yan, Ceramic laser materials. *Nat. Photonics* **2**, 721–727 (2008)
2. R. Komatsu, T. Sugawara, K. Sassa, Growth and ultraviolet application of $\text{Li}_2\text{B}_4\text{O}_7$ crystals: generation of the fourth and fifth harmonics of Nd:Y₃Al₅O₁₂ lasers. *Appl. Phys. Lett.* **70**, 3492 (1997)
3. J. Lu, H. Yagi, K. Takaichi, T. Uematsu, J.F. Bisson, Y. Feng, A. Shirakawa, K.I. Ueda, T. Yanagitani, A.A. Kaminskii, 110 W ceramic Nd³⁺:Y₃Al₅O₁₂ laser. *Appl. Phys. B* **79**, 25–28 (2004)
4. J.R. Lu, K. Ueda, H. Yagi, T. Yangitani, Y. Akiyama, A. AKaminskii, Neodymium doped yttrium aluminum garnet (Y₃Al₅O₁₂) nanocrystalline ceramics—a new generation of solid state laser and optical materials. *J. Alloy Comps.* **341**, 220–225 (2002)
5. R.J. Ralph, F.K. William, J.W. Marvin, Measurement of excited-state-absorption loss for Ce³⁺ in Y₃Al₅O₁₂ and implications for tunable 5d-4f rare-earth lasers. *Appl. Phys. Lett.* **33**, 410 (2008)
6. F.W. Kang, X.B. Yang, M.Y. Peng, L. Wondraczek, Z.J. Ma, Q.Y. Zhang, J.R. Qiu, Red photoluminescence from Bi³⁺ and the influence of the oxygen vacancy perturbation in ScVO₄: a combined experimental and theoretical study. *J. Phys. Chem. C* **118**, 7515–7522 (2014)
7. M. Dorogova, A. Navrotsky, L.A. Boatner, Enthalpies of formation of rare earth orthovanadates, REVO₄. *J. Solid State Chem.* **180**, 847–851 (2007)
8. I.L. Snetkov, D.E. Silin, O.V. Palashov, E.A. Khazanov, H. Yagi, T. Yanagitani, H. Yoneda, A. Shirakawa, K. Ueda, A.A. Kaminskii, Thermo-optical constants of sesquioxide laser ceramics Yb³⁺:Ln₂O₃ (Ln = Y, Lu, Sc). *Phys. Status Solidi A* **210**, 907–913 (2013)
9. X.M. Zhang, Z.W. Quan, J. Yang, P.P. Yang, H.Z. Lian, J. Lin, Solvothermal synthesis of well-dispersed MF₂ (M = Ca, Sr, Ba) nanocrystals and their optical properties. *Nanotechnology* **19**, 075603 (2008)
10. K. Niwa, Y. Furukawa, S. Takekawa, K. Kitamura, Growth and characterization of MgO doped near stoichiometric LiNbO₃ crystals as a new nonlinear optical material. *J. Cryst. Growth* **208**, 493–500 (2000)
11. R. Reisfeld, D. Brusilovsky, M. Eyal, E. Miron, Z. Burstein, J. Ivri, A new solid-state tunable laser in the visible. *Chem. Phys. Lett.* **160**, 43–44 (1989)
12. C. Czeranowsky, E. Heumann, G. Huber, All-solid-state continuous-wave frequency-doubled Nd:YAG-BiBO laser with 2.8-W output power at 473 nm. *Opt. Lett.* **28**, 432–434 (2003)
13. D.A. Rockwell, A review of phase-conjugate solid-state lasers. *IEEE J Quantum Elect.* **24**, 1124–1140 (1988)
14. J.J. Zayhowski, A. Mooradian, Single-frequency microchip Nd lasers. *Opt. Lett.* **14**, 24–26 (1989)
15. B. Liu, J. Li, R. Yavetskiy, Fabrication of YAG transparent ceramics using carbonate precipitated yttria powder. *J. Eur. Ceram. Soc.* **35**, 2379–2390 (2015)
16. L. Wen, X. Sun, Z. Xiu, Synthesis of nanocrystalline yttria powder and fabrication of transparent YAG ceramics. *J. Eur. Ceram. Soc.* **24**, 2681–2688 (2004)
17. P.V. Lu, Ceramic laser materials and the prospect for high power lasers. *Opt. Mater.* **31**, 701–706 (2009)
18. F. Rivera-López, P. Babu, C. Basavapoorima, C.K. Jayasankar, V. Lavín, Efficient Nd³⁺ → Yb³⁺ energy transfer processes in high phonon energy phosphate glasses for 1.0 μm Yb³⁺ laser. *J. Appl. Phys.* **109**, 123514 (2011)
19. A.D. Pearson, S.P.S. Porto, Nonradiative energy exchange and laser oscillation in Yb³⁺, Nd³⁺ doped borate glass. *Appl. Phys. Lett.* **4**, 202 (2004)
20. R. Balda, J. Fernández, I. Iparraguirre, M. Al-Saleh, Spectroscopic study of Nd³⁺/Yb³⁺ in disordered potassium bismuth molybdate laser crystals. *Opt. Mater.* **28**, 1247–1252 (2006)
21. G.E. Peterson, A.D. Pearson, P.M. Bridenbaugh, Energy exchange from Nd³⁺ to Yb³⁺ in calibo glass. *Appl. Phys. Lett.* **36**, 1962 (2004)
22. L.H. Ahrens, The use of ionization potentials Part 1. Ionic radii of the elements. *Geochim. Cosmochim. Acta* **2**, 155–169 (1952)
23. R.D. Shannon, Revised effective ionic radii and systematic studies of interatomic distances in halides and chalcogenides. *Acta Crystallogr. A* **A32**, 751–767 (1976)
24. T.P. Xie, L. Zhang, Y. Guo, X.X. Wang, Y.J. Wang, Tuning of Bi³⁺-related excitation and emission positions through crystal field modulation in the perovskite-structured La₂(Zn_xMg_{1-x})TiO₆ (0 ≤ x ≤ 1):Bi³⁺ solid solution for white LEDs. *Ceram. Int.* (2018). <https://doi.org/10.1016/j.ceramint.2018.10.262>
25. Z.G. Xia, C.G. Ma, M.S. Molokeev, Q.L. Liu, K. Rickert, K.R. Poeppelmeier, Chemical unit cosubstitution and tuning of photoluminescence in the Ca₂(Al_{1-x}Mg_x)(Al_{1-x}Si_{1+x})O₇:Eu²⁺ phosphor. *J. Am. Chem. Soc.* **137**, 12494–12497 (2015)
26. S. Kostić, Z. Lazarević, V. Radojević, Study of structural and optical properties of YAG and Nd:YAG single crystals. *Mater. Res. Bull.* **63**, 80–87 (2015)
27. L.J. Liu, H. Zhou, S.Q. Dong, Raman spectroscopy of sulfur structure in borosilicate waste glasses. *At. Energy Sci. Technol.* **43**, 103–107 (2009)
28. G. Antoine, Infrared (2–12 μm) solid-state laser sources: a review. *C. R. Phys.* **8**, 1100–1128 (2007)
29. L.I. Ivleva, T.T. Basiev, I.S. Voronina, P.G. Zverev, V.V. Osiko, N.M. Polozkov, SrWO₄:Nd³⁺ – new material for multifunctional lasers. *Opt. Mater.* **23**, 439–442 (2003)
30. C. Maunier, J.L. Doualan, R. Moncorgé, A. Speghini, M. Bettinelli, E. Cavalli, performance of Nd:LuVO₄ a new infrared laser material that is suitable for diode pumping. *J. Opt. Soc. Am. B* **19**, 1794–1800 (2002)
31. W.B. Chen, Y. Inagawa, T. Omatsu, M. Tateda, N. Takeuchi, Y. Usuki, Diode-pumped, self-stimulating, passively Q-switched Nd³⁺:PbWO₄ Raman laser. *Opt. Commun.* **194**, 401–407 (2001)
32. S. Singh, D.C. Miller, J.R. Potopowicz, L.K. Shick, Emission cross section and fluorescence quenching of Nd³⁺ lanthanum pentaphosphate. *J. Appl. Phys.* **46**, 1191 (1975)
33. R. Balda, J. Fernandez, A. Mendioroz, J.L. Adams, B. Boulard, Temperature-dependent concentration quenching of Nd³⁺ fluorescence in fluoride glasses. *J. Phys.* **6**, 913 (1994)
34. C. Koepke, K. Wisniewski, L. Sikorski, D. Piatkowski, K. Kowalska, M. Naftaly, Upconverted luminescence under 800 nm laser diode excitation in Nd³⁺-activated fluoroaluminate glass. *Opt. Mater.* **28**, 129–136 (2006)
35. A.A. Andrade, T. Catunda, R. Lebullenger, A.C. Hernandez, M.L. Baesso, Thermal lens measurements of fluorescence

- quantum efficiency in Nd³⁺-doped fluoride glasses. *J. Non-Cryst. Solids* **284**, 255–260 (2001)
36. D. Singh, V. Tanwar, S. Bhagwan, I. Singh, Recent advances in luminescent materials and their potential applications, in *Advanced Magnetic and Optical Materials* (Wiley, 2016), pp. 317–352
 37. D. Singh, V. Tanwar, A.P. Simantilleke, B. Mari, P.S. Kadyan, I. Singh, Rapid synthesis and enhancement in down conversion emission properties of BaAl₂O₄:Eu²⁺, RE³⁺ (RE³⁺ = Y, Pr) nanophosphors. *J. Mater. Sci. Mater. Electron.* **27**, 2260–2266 (2016)
 38. Z.G. Xia, Q.L. Liu, Progress in discovery and structural design of color conversion phosphors for LEDs. *Prog. Mater. Sci.* **84**, 59–117 (2016)
 39. L. Wang, R.J. Xie, T. Suehiro, T. Takeda, N. Hirosaki, Down-conversion nitride materials for solid state lighting: recent advances and perspectives. *Chem. Rev.* **118**, 1951–2009 (2018)
 40. F. Wang, X.G. Liu, Lanthanide-doped luminescent nanoprobe: controlled synthesis, optical spectroscopy, and bioapplications. *Chem. Soc. Rev.* **38**, 976–989 (2009)
 41. F.W. Kang, J.J. He, T.Y. Sun, Z.Y. Bao, F. Wang, D.Y. Lei, Plasmonic dual-enhancement and precise color tuning of gold nanorod@SiO₂ coupled core-shell-shell upconversion nanocrystals. *Adv. Funct. Mater.* **27**(36), 1701842 (2017)
 42. Y. Liu, D. Tu, H. Zhu, X. Chen, Lanthanide-doped luminescent nanoprobe: controlled synthesis, optical spectroscopy, and bioapplications. *Chem. Soc. Rev.* **42**, 6924–6958 (2013)